# Measuring the Optical Concurrence of Vector Beams with an Atomic-State Interferometer

Jinwen Wang,[1,2,*] Sphinx J. Svensson,[2] Thomas W. Clark,[3] Yun Chen,[1,4] Mustafa A. Al Khafaji,[2,5] Hong Gao,[1,†] Niclas Westerberg,[2] and Sonja Franke-Arnold[2,‡]

[1]*Ministry of Education Key Laboratory for Nonequilibrium Synthesis and Modulation of Condensed Matter, Shaanxi Province Key Laboratory of Quantum Information and Quantum Optoelectronic Devices, School of Physics, Xi'an Jiaotong University, Xi'an 710049, China*

[2]*School of Physics and Astronomy, University of Glasgow, G12 8QQ, United Kingdom*

[3]*HUN REN Wigner Research Centre for Physics, Budapest H-1525, Hungary*

[4]*School of Science, Huzhou University, Zhejiang Huzhou 313000, China*

[5]*Fraunhofer CAP, Glasgow, G1 1RD, United Kingdom*

(Received 26 May 2023; accepted 3 April 2024; published 9 May 2024)

We investigate the transmission of vector beams, correlated in their polarization and spatial degrees of freedom, through cold atoms in the presence of a transverse magnetic coupling field. The resulting phase-dependent dynamics allow us to imprint the spatially varying polarization of a vector beam onto atomic spin polarizations, thereby establishing a direct link between optical space-polarization correlations and atomic-state interference. We find that the resulting absorption profiles show interference fringes whose modulation strength is given by the squared concurrence of the vector beam, letting us identify optical concurrence from a single absorption image. We expect impact across a diverse range of applications, including spintronics, quantum memories, metrology, and clocks.

DOI: 10.1103/PhysRevLett.132.193803

*Introduction.*—Optical information can be encoded in the polarization degree of freedom, parametrized by the optical spin, and in the spatial degree of freedom, i.e., the phase and intensity profile of the transverse optical modes [1,2]. Vector beams combine both polarization and spatial information. Composed of orthogonal polarization components with different complex amplitudes, they exhibit spatially varying polarization profiles, offering a wide range of applications [3–5]. Atomic dipole transitions are sensitive to polarization via selection rules, and to the complex light amplitude via the Rabi frequency, making atoms active optical elements that can modify and be modified by the intrinsic properties of vector beams. This two-way interaction allows for the creation of complex optical phenomena, which have been studied extensively over the last few decades [6]. Vectorial light-atom interaction can generate spatial anisotropy [7–9] and coherence [10–12] in atoms, and tailor nonlinear effects [13–16]. Vector beams have also been stored [17,18] and converted [19,20] in atomic systems.

In this Letter, we establish, theoretically and experimentally, a direct link between polarization-spatial correlations of light and atomic-state interference, which can be expressed as an uncommonly simple relationship between fringe visibility and optical concurrence. We investigate the transmission of vector beams through an atomic gas, and demonstrate that the degree of correlation between the polarization and spatial degree of freedom, i.e., the "vectorness," or optical concurrence [21–24], influences the light-matter interaction. Specifically, we show that the resulting absorption profile contains interference fringes, whose visibility is determined by the concurrence. We can therefore identify the optical concurrence from a single absorption measurement, whereas conventional all-optical measurements require at least four, more commonly six, measurements [23].

We realize an atomic-state interferometer in cold $^{87}$Rb formed by a vector beam driving a two-photon $\Lambda$ transition between two Zeeman sublevels, which are coupled by a transverse magnetic field (TMF). The atomic medium effectively allows us to "interfere" optical amplitudes encoded in the orthogonal polarization components, thereby converting concurrence to intensity modulation. Interaction with the vector beam establishes spatially varying spin polarizations in the atomic medium, which in turn modify the transmitted light. Through spatial analysis of the resulting absorption pattern, we can quantify this dependency and identify the optical concurrence. Recent work [25] has

demonstrated a similar transfer of vector beams to the spatial spin texture in a semiconductor quantum well, leading to rotating spin waves. Both quantum wells and atomic gasses are promising candidates for spintronics, offering interfaces for the storage and manipulation of the high-dimensional state space provided by vector light fields.

*Concept and theoretical model.*—Every paraxial vector beam (with $E_z = 0$) can be expressed as $\mathbf{E}(\mathbf{r}_\perp) = u_1(\mathbf{r}_\perp)\boldsymbol{\sigma}_1 + u_2(\mathbf{r}_\perp)\boldsymbol{\sigma}_2$, where $\mathbf{r}_\perp$ denotes the transverse position, $u_i$ ($\forall\ i \in 1, 2$) are complex spatial modes, and $\boldsymbol{\sigma}_i$ are orthogonal polarization directions. Homogeneously polarized light can be expressed as a product state $u\boldsymbol{\sigma}$, whereas orthogonal spatial modes $u_1 \perp u_2$ signify maximal correlations between the spatial and polarization degrees of freedom. The nonseparability is captured by the concurrence [23]

$$C = 2\sqrt{(u_1, u_1)(u_2, u_2) - (u_1, u_2)^2}, \tag{1}$$

which ranges from 0, for homogeneous polarization, to 1, for maximal correlation. Here, $(u_i, u_j) = \int d\mathbf{r}_\perp u_i^*(\mathbf{r}_\perp) u_j(\mathbf{r}_\perp)$ denotes the spatially averaged (global) scalar product between the participating spatial light modes. An alternative expression, in terms of the experimentally accessible global Stokes parameters, is $C = \sqrt{1 - (S_1^2 + S_2^2 + S_3^2)/S_0^2}$, where $S_0$ is the total intensity, $S_1$ describes the intensity difference between horizontal and vertical, $S_2$ between diagonal and antidiagonal, and $S_3$ between right and left circular polarization components.

We illustrate our method for vector beams of the form

$$\mathbf{E} = E(r)[\sin(\chi) e^{-i\psi} e^{-i\ell\varphi}\boldsymbol{\sigma}_+ + \cos(\chi) e^{i\psi} e^{i\ell\varphi}\boldsymbol{\sigma}_-]. \tag{2}$$

Here, the polarization is defined in terms of right and left circular components $\boldsymbol{\sigma}_\pm$ to facilitate mapping to the usual atomic bases. The spatial degree of freedom is addressed by transverse light modes with equal and opposite orbital angular momentum (OAM) $\exp(\pm i\ell\varphi)$ and varying amplitudes. The orthogonal states $\exp(\pm i\ell\varphi)\boldsymbol{\sigma}_\mp$ then form the poles of a high-order Poincaré sphere (HOPS, Fig. 1) [26], where the polar angle $\chi \in [0, \pi/2]$ controls the relative amplitude, and the azimuthal angle $\psi \in [0, \pi]$ changes the relative phase. The former is responsible for changing the degree of spin-orbit correlation. When $\chi = \pi/4$, states lie on the equator and contain spatially varying linear polarizations which rotate as a function of the azimuthal angle $\psi$. These show maximal spin-orbit correlations. States located at the poles ($\chi = 0$ or $\chi = \pi/2$) are homogeneously right or left circularly polarized and hence fully separable in their polarization and spatial degrees of freedom. More generally, from Eqs. (1) and (2), we can identify the concurrence as

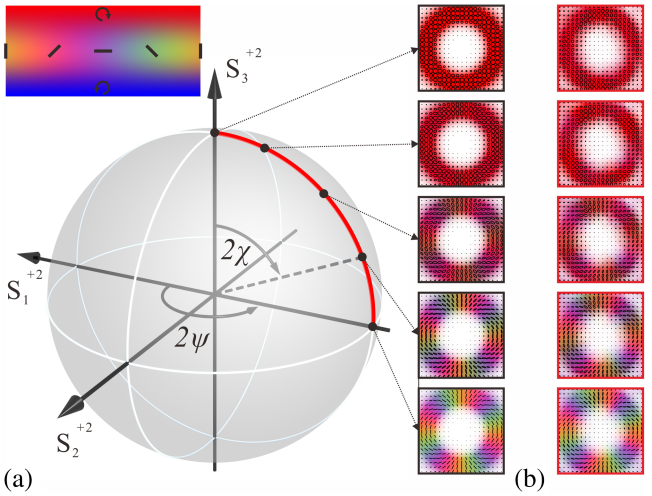


FIG. 1. (a) Schematic illustration of the HOPS with $\boldsymbol{\sigma}_\pm e^{\mp i2\varphi}$ forming the poles and simulated vector beams located along the red line with $2\psi = \pi$, and $2\chi = 0$, $\pi/10$, $7\pi/30$, $11\pi/30$, and $\pi/2$. (b) Corresponding experimentally generated vector beams. The inset on the top left shows our color encoding for the different polarization states.

$$C = \sin(2\chi). \tag{3}$$

The $\boldsymbol{\sigma}_\pm$ components in Eq. (2) couple atomic transitions between magnetic states with $\Delta m_F = \pm 1$. For a suitable atomic system, these transitions can be closed either optically [10] or magnetically [27], facilitating phase-coherent atomic dynamics. The $\boldsymbol{\sigma}_\pm$ transitions then act as two arms within an atomic-state interferometer, rendering the atomic response sensitive to the phase difference imposed by the complex light amplitudes driving these transitions. For spatially varying phase differences, like in our vector beams, the atomic response then also varies spatially, which manifests as fringes in the absorption profile. Changing the relative weighting between the transition channels will change the fringe visibility, thus linking polarization modulation (optical concurrence) to intensity modulation (the visibility of interference fringes).

In the following text, we model the transmission of vector beams, with varying concurrence, through cold atoms using both optical Bloch (OB) equations and partially dressed perturbation theory. The latter results in a concise analytical formula for the transmission profile, with fringe visibility determined by the optical concurrence.

In line with our experiment, we consider a standard Zeeman configuration for the $F = 1 \rightarrow F' = 0$ transition driven by a weak, resonant vector probe beam [Eq. (2)] in the perturbative regime and in the presence of a static $\mathbf{B}$ field along the $x$ axis, as shown in the inset of Fig. 2. The quantization axis is set along the light propagation direction. Thus, we obtain an atomic-state interferometer connecting the $F = 1$, $m_F = \pm 1$ Zeeman sublevels $|\pm 1\rangle$ via the $F' = 0$, $m'_F = 0$ excited state $|e\rangle$ in a $\Lambda$-type optical

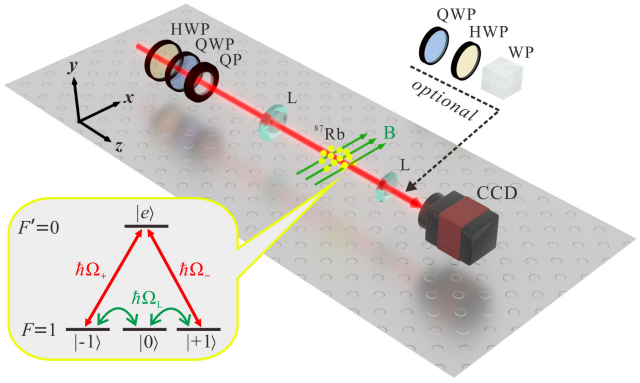


FIG. 2. Simplified experimental setup. Optical elements for vector beam generation and analysis: HWP, half wave plate; QWP, quarter wave plate; QP, q plate; L, lens; B, magnetic field; WP, Wollaston prism; CCD, charge-coupled device. The bottom left inset shows the atomic level scheme indicating the Λ transition driven by the vector beam and transverse magnetic coupling.

transition by orthogonal circular polarization components with opposite OAM and by magnetic coupling due to the TMF. The Hamiltonian of the system in the Zeeman basis under the rotating wave approximation is

$$\hat{H}_Z/\hbar = -\Omega_L|\pm 1\rangle\langle 0|/\sqrt{2} - \Omega_\pm|\pm 1\rangle\langle e| + \text{H.c.}, \quad (4)$$

where $\Omega_L = g_F\mu_B|\mathbf{B}|$ is the Larmor frequency, $g_F$ the Landé $g$ factor, and $\mu_B$ the Bohr magneton. The parameters $\Omega_\pm$ denote the optical coupling with

$$\Omega_\pm = \frac{\Omega_R}{2\sqrt{3}}\left\{\begin{matrix}\cos(\chi)\\ \sin(\chi)\end{matrix}\right\}e^{\pm i(\ell\varphi+\psi)}, \quad (5)$$

where $\Omega_R = E(r)\boldsymbol{\sigma}_\pm \cdot \mathbf{d}_{e\pm}$ is the Rabi frequency, with $\mathbf{d}_{e\pm}$ being the transition dipole moments for the $\boldsymbol{\sigma}_\pm$ polarization, respectively, and the factor of $1/\sqrt{3}$ originates from appropriate Wigner-Eckart coefficients [28].

We first consider the OB model for the Zeeman basis Hamiltonian [Eq. (4)]. In conjunction with terms describing relaxation $\hat{\Gamma} = \sum_i \gamma|i\rangle\langle i| + (\gamma+\Gamma)|e\rangle\langle e|$ and repopulation $\hat{\Lambda} = \sum_i \frac{1}{3}(\gamma + \Gamma\hat{\rho}_{e,e})$, where $\Gamma$ represents the spontaneous emission and $\gamma$ the transit decay rate, we obtain the Liouville equations [29]:

$$\frac{d}{dt}\hat{\rho} = -\frac{i}{\hbar}[\hat{H}_Z, \hat{\rho}] - \frac{1}{2}(\hat{\Gamma}\hat{\rho} + \hat{\rho}\hat{\Gamma}) + \hat{\Lambda}. \quad (6)$$

Solving the Liouville equation (Bloch equations) numerically under the steady-state condition [30–32], we obtain the atomic absorption through the steady-state excited state population $\rho_{ee}(t \to \infty)$; see Supplemental Material [33].

To develop physical understanding of the dynamics, we rewrite the Zeeman basis Hamiltonian [Eq. (4)] in a partially dressed state basis. We define the coupling, noncoupling, and intermediate states, respectively, as

$$\begin{aligned}
|\psi_C\rangle &= e^{-i(\ell\varphi+\psi)}\sin\chi|+1\rangle + e^{i(\ell\varphi+\psi)}\cos\chi|-1\rangle,\\
|\psi_{NC}\rangle &= -e^{-i(\ell\varphi+\psi)}\cos\chi|+1\rangle + e^{i(\ell\varphi+\psi)}\sin\chi|-1\rangle,\\
|\psi_1\rangle &= [-\sin(2\chi)|\psi_{NC}\rangle - J|0\rangle]/N,\\
|\psi_2\rangle &= [J^*|\psi_{NC}\rangle - \sin(2\chi)|0\rangle]/N, \quad (7)
\end{aligned}$$

where the normalization constant is defined by $N^2(\chi,\varphi) = [1+\cos(2\ell\varphi+2\psi)\sin 2\chi]/2$ and, for notational convenience, $J = [e^{-i(\ell\varphi+\psi)}\sin\chi + e^{+i(\ell\varphi+\psi)}\cos\chi]/\sqrt{2}$ and $\bar{J} = [-e^{+i(\ell\varphi+\psi)}\cos\chi + e^{-i(\ell\varphi+\psi)}\sin\chi]/\sqrt{2}$. When expressed in the basis of $|e\rangle$, $|\psi_C\rangle$, $|\psi_1\rangle$, and $|\psi_2\rangle$, the Hamiltonian takes the form

$$\begin{aligned}
\frac{\hat{H}_D}{\hbar} = &-\frac{\Omega_R}{2\sqrt{3}}|\psi_C\rangle\langle e| + \Omega_L N(\chi,\varphi)|\psi_C\rangle\langle\psi_1|\\
&+ \Omega_L\frac{\bar{J}^*(\chi,\varphi)[J^*(\chi,\varphi)]^2}{N^2(\chi,\varphi)}|\psi_1\rangle\langle\psi_2| + \text{H.c.} \quad (8)
\end{aligned}$$

The rate at which the light induces a transition between the dark state $|\psi_2\rangle$ and the excited state $|e\rangle$ is then given to third order in perturbation theory (PT) as

$$\begin{aligned}
T_{2\to e} &\propto |\langle e|\hat{H}_D|\psi_C\rangle\langle\psi_C|\hat{H}_D|\psi_1\rangle\langle\psi_1|\hat{H}_D|\psi_2\rangle|^2\\
&\propto \Omega_L^4\Omega_R^2[1-\sin^2(2\chi)\cos^2(2\ell\varphi+2\psi)]. \quad (9)
\end{aligned}$$

The transition rate shows a $2\ell$-fold rotational symmetry and depends on the angles $\psi$ and $\chi$, which characterize the vector beam on the HOPS. Transitions at certain angular positions within the beam $\varphi$ will be suppressed, resulting in interference fringes. Remarkably, we can identify their modulation

$$\mathcal{M} = \frac{\max(T_{2\to e}) - \min(T_{2\to e})}{\max(T_{2\to e})} = \sin^2(2\chi) \quad (10)$$

with the concurrence of Eq. (3). For a beam with maximal concurrence ($\chi = \pi/4$), the transition rate vanishes at certain angular positions, so that $|\psi_2\rangle$ becomes a dark state in which light and atoms do not interact and the atoms are rendered transparent. The absorption pattern will therefore show interference fringes with maximal visibility. If $\chi$ deviates from this value, the modulation of the transmission and the resulting fringe visibility will decrease and vanish for homogeneously polarized light. This indicates that the concurrence can be identified from a single atomic absorption profile, a result that should hold beyond the specific example considered here. We note that a rotation of the polarization profile by $2\psi$ rotates the transmission rate and absorption profile by the same angle, in agreement with our previous work [34,35]. Naturally, PT is limited in its

applicability, and is unsuitable for strong interactions or appreciable dissipation. In the following section, we compare the two models with the experimental results.

*Experimental realization and discussion.*—Our simplified experimental setup is shown in Fig. 2. A cold cloud of $^{87}$Rb atoms was collected in a magneto-optical trap and spatially compressed by a dark spontaneous-force optical trap (SpOT) following the experimental procedure outlined in [36]. For the current work, approximately $3 \times 10^7$ atoms were prepared in the SpOT, distributed equally over the $F = 1$ ground states. The atomic cloud expanded freely for 3.5 ms, reaching an average atomic density of $2 \times 10^{10}$ cm$^{-3}$ and a temperature of 100 μK before interaction with the probe beam. The background magnetic field was canceled, and a TMF $\mathbf{B}$ was added along the $x$ axis with a fixed magnitude of 1 G using three orthogonal sets of rectangular coils. The frequency of the vector beam was locked to the $F = 1 \rightarrow F' = 0$ transition of the $D_2$ line, and its power set to 0.20 μW (corresponding to an intensity of 0.052 mW/cm$^2$ in the area of interest).

The vector beam was generated by an $\ell = +2$ vortex retarder, and the beam evolution on the HOPS was realized by the combination of a half and quarter wave plate, whose rotations control the polar angle $\chi$ and the azimuth $\psi$ in Eq. (2), respectively. To identify the polarization structure of the beam, we perform full spatially resolved Stokes tomography using the set of (optional) optical components shown in Fig. 2. These measurements also allow us to identify the optical concurrence. Setting $2\psi = \pi$ and increasing $\chi$ from 0 to $\pi/4$ generates vector beams with a concurrence ranging from 0 to 1. A selection of measured polarization and intensity profiles is shown in Fig. 1(b), alongside the corresponding simulated vector beams in Fig. 1(a). As the orthogonal polarization components do not interfere, the intensity profile has the typical doughnut shape of OAM beams.

We explore the atomic transmission of these vector beams by measuring changes to the light intensity after interaction. For each vector beam, images of the light profile are recorded with a CCD in the presence of atoms ($I_{\text{atoms}}$), in the absence of atoms ($I_{\text{probe}}$), and without lasers ($I_{\text{dark}}$) (the latter to subtract spurious light signals unrelated to the experiment). In the Supplemental Material [33], we show the recorded intensity and polarization structures after interaction with the atoms, which indicate that the atomic response is determined by the interplay between the local polarization direction and the TMF. The spatially varying optical attenuation is more clearly expressed by the optical density (OD),

$$\text{OD} = \ln \frac{I_{\text{probe}} - I_{\text{dark}}}{I_{\text{atoms}} - I_{\text{dark}}}, \tag{11}$$

as this yields a measure of the total absorption [37], effectively visualizing interference of the transition

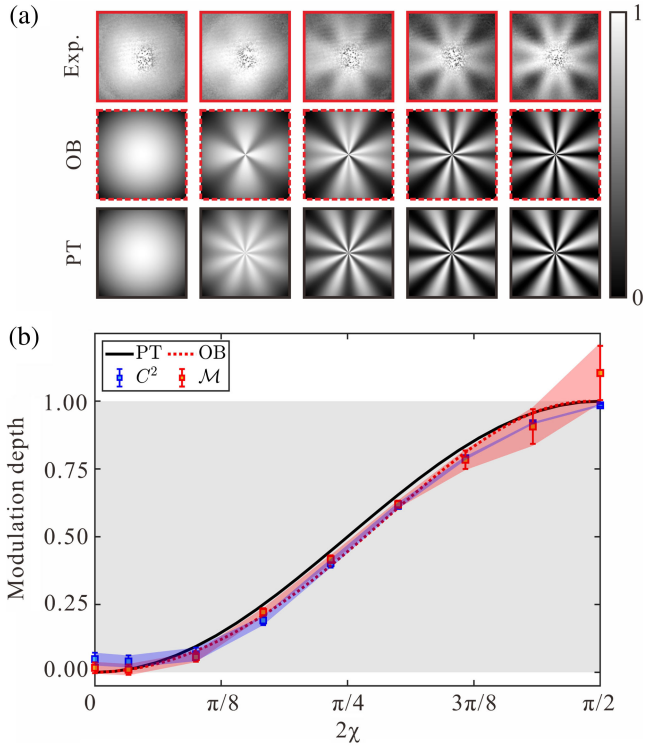


FIG. 3. (a) Measured and predicted peak-normalized OD images ($0.8 \times 0.8$ mm$^2$) for selected beams with increasing concurrence [see Fig. 1(b)], with high (low) OD corresponding to beam areas of large (small) absorption. (b) The equivalence between the squared concurrence of the vector beam and the modulation depth $\mathcal{M}$ of the atomic absorption profile as a function of $2\chi$. The black line shows $\mathcal{M}$ according to the PT model, which is identical to $C^2$ of the target vector beams. The measured $C^2$ values are shown in blue, and the measured $\mathcal{M}$ in red, with error bars representing the standard deviation of five runs. The dashed red line indicates $\mathcal{M}$ according to the OB model.

amplitudes in our atomic-state interferometer. Measured OD images for the selection of vector beams displayed in Fig. 1(b) are shown in the top row of Fig. 3(a), and additional experimental results for the full range of $2\chi \in \{0, \pi\}$ can be found in the Supplemental Material [33]. As predicted by Eq. (9), an increase in concurrence is associated with a larger variation in the transmission.

According to Eq. (9), and for $\ell = 2$ and $2\psi = \pi$, the transition rate $T_{2\rightarrow e}$ is minimal when $\varphi = n\pi/4 \ \forall \ n \in \mathcal{Z}$. This corresponds to positions where the polarization is parallel or perpendicular to the external (horizontal) magnetic field. Here, the population of $|\psi_2\rangle$ is rapidly repopulated by incoherent decay, rendering the atoms more transparent to the light and leading to a reduced OD. We compare our data with simulations according to the OB model and analytical results from the PT model. The parameters for all calculations, in accordance with experiment, are $\Gamma = 2\pi \times 6$ MHz, $\gamma = 10^{-7}\ \Gamma$, $\Omega_L = 0.02\ \Gamma$, $\Omega_R = 0.1\ \Gamma$, and $\ell = 2$. In the middle row of Fig. 3(a)

we plot $\rho_{ee}(\mathbf{r}_\perp)$, which is a good measure of the transmission amplitude, and in the lower row we show the normalized transition rate $T_{2\to e}$. While the simple analytical expression obtained via PT gives a reasonable qualitative explanation of the physical processes, it does not include a quantitative description of decoherence, and in particular it does not explain the difference in modulation at positions where the polarization is parallel or perpendicular to $\mathbf{B}$. We expect this to be a higher-order effect not captured by third-order perturbation theory. Analysis based on the full Liouville equations, however, gives better agreement with the experimental data but lacks a simple analytical explanation.

Qualitatively, our results confirm that the absorption pattern, specifically the modulation of the fringe visibility, depends strongly on the beam concurrence. The atoms respond uniformly to circularly polarized light, whereas they become transparent to areas of vector beams where the polarization axis is parallel or orthogonal to the applied magnetic field, thus producing structured OD patterns with distinct fringe visibility. We examine this quantitatively in Fig. 3(b) by showing the equivalence of the squared optical concurrence of the input vector beam to the fringe modulation of the absorption pattern. According to PT, the modulation of the transmission rate between $|\psi_2\rangle \to |e\rangle$ is given by $\mathcal{M} = \sin^2(2\chi)$, which is identical to the squared concurrence of the vector beam displayed as a black line. We compare these with measurements of the optical concurrence and of the fringe modulation obtained from the OD data. For each vector beam with a specific target value of $2\chi$, we identified the concurrence based on Stokes tomography, and plotted the measured $C^2$ values as blue disks in Fig. 3(b). These deviate slightly from the target values due to small imperfections in beam generation and the tomography process. Measured values consistently exceed the target value, especially for small values of $C$, which would be a natural result of optical noise. While the fringe visibility according to the PT model is a simple geometric function, for experimental data, as well as for simulation via the OB model, it has to be extracted numerically. We note that, for our vector beams, the modulation strength $\mathcal{M}$ is identical to the $\ell = 2$ Fourier coefficient of the transition amplitude $T_{2\to e}$, and it can therefore be extracted by a Fourier series expansion [34]. Applying this method to the experimental data allows us to average over the different peaks, thereby reducing the effect of noise. The resulting values for $\mathcal{M}$ are shown as red squares in Fig. 3(b). Similarly, we obtain a corresponding theoretical $\mathcal{M}$ from simulations of the excited state population based on our OB model shown as a dashed red line. We find that the model based on the OB equations deviates slightly from the PT model and is in excellent agreement with the data. Overall, the results confirm that we can identify vector beam concurrence from a single absorption image.

*Conclusions.*—We demonstrated how to map the concurrence of vector beams to steady-state populations and transitions in an atomic cloud. An atomic-state interferometer was constructed by combining optical coupling via vector beams and magnetic coupling in an external TMF. This allowed us to transfer the correlations between the spin and spatial degree of freedom present in vector beams to spatially varying spin polarizations in atoms, which in turn led to spatially varying absorption patterns. More specifically, we derived theoretically and demonstrated in experiment that the visibility of the fringe pattern in the absorption profile is given by the squared concurrence of the vector beam. This illustrates the direct impact of correlations between the spatial and polarization degree of freedom of light on atomic-state interference.

In the current setup, an atomic-state interferometer was constructed by combining magnetic and optical coupling in a degenerate two-level system. Other coupling methods, e.g., microwave coupling [38], may expand such an interaction to bichromatic fields. Our demonstration was performed for a specific form of simple vector beams, but the principle may be generalized to arbitrary vector modes, such as topological light [39–41] or optical lattices [42–44]. The proposed scheme provides an effective approach for information transfer and manipulation of vector beams in atomic systems, and potentially the control of entanglement between atoms and polarization-structured photons. The degree of correlation between polarization and spatial degrees of freedom may be transferred to the internal state of the atoms, offering opportunities for a new branch of vectorial light-matter interaction that may be extended to atomic BECs [45–47], ions [48,49], or molecules [50].

S. F.-A., N. W. and T. W. C. acknowledge support through the QuantERA II Programme, with funding received via the EU H2020 research and innovation programme under Grant No. 101017733, S. F.-A. and N. W. acknowledge associated support from EPSRC under Grant No. EP/Z000513/1 (V-MAG). T. W. C. acknowledges support by the National Research, Development and Innovation Office of Hungary within the Quantum Technology National Excellence Program (Project No. 2017-1.2.1-NKP-2017-00001). N. W. wishes to acknowledge support from the Royal Commission for the Exhibition of 1851. J. W. acknowledges support by the China Scholarship Council (Grant No. 201906280228). This work is also supported by the National Natural Science Foundation of China (Grant No. 92050103), the Postdoctoral Fellowship Program of China Postdoctoral Science Foundation (Grant No. GZC20232118), the Shaanxi Province postdoctoral Science Foundation (Grant No. 2023BSHEDZZ23) and the Fundamental Research Funds for the Central Universities (Grant No. xzy012023042).

*jinwenwang@xjtu.edu.cn
†honggao@xjtu.edu.cn
‡sonja.franke-arnold@glasgow.ac.uk

[1] S. Franke-Arnold, Phil. Trans. R. Soc. A **375**, 20150435 (2017).
[2] M. Babiker, D. L. Andrews, and V. E. Lembessis, J. Opt. **21**, 013001 (2018).
[3] Q. Zhan, Adv. Opt. Photonics **1**, 1 (2009).
[4] C. Rosales-Guzmán, B. Ndagano, and A. Forbes, J. Opt. **20**, 123001 (2018).
[5] Y. Shen and C. Rosales-Guzmán, Laser Photonics Rev. **16**, 2100533 (2022).
[6] J. Wang, F. Castellucci, and S. Franke-Arnold, AVS Quantum Sci. **2**, 031702 (2020).
[7] F. K. Fatemi, Opt. Express **19**, 25143 (2011).
[8] J. Wang, X. Yang, Y. Li, Y. Chen, M. Cao, D. Wei, H. Gao, and F. Li, Photonics Res. **6**, 451 (2018).
[9] J. Wang, X. Yang, Z. Dou, S. Qiu, J. Liu, Y. Chen, M. Cao, H. Chen, D. Wei, K. Müller-Dethlefs *et al.*, Appl. Phys. Lett. **115**, 221101 (2019).
[10] S. Barreiro, J. W. R. Tabosa, H. Failache, and A. Lezama, Phys. Rev. Lett. **97**, 113601 (2006).
[11] N. Radwell, T. W. Clark, B. Piccirillo, S. M. Barnett, and S. Franke-Arnold, Phys. Rev. Lett. **114**, 123603 (2015).
[12] X. Yang, Y. Chen, J. Wang, Z. Dou, M. Cao, D. Wei, H. Batelaan, H. Gao, and F. Li, Opt. Lett. **44**, 2911 (2019).
[13] S. Shi, D.-S. Ding, Z.-Y. Zhou, Y. Li, W. Zhang, and B.-S. Shi, Appl. Phys. Lett. **106**, 261110 (2015).
[14] F. Bouchard, H. Larocque, A. M. Yao, C. Travis, I. De Leon, A. Rubano, E. Karimi, G.-L. Oppo, and R. W. Boyd, Phys. Rev. Lett. **117**, 233903 (2016).
[15] H. Hu, D. Luo, C. Pan, Y. Qin, Y. Zhang, D. Wei, H. Chen, H. Gao, and F. Li, Opt. Lett. **46**, 2614 (2021).
[16] A. N. Black, S. Choudhary, E. S. Arroyo-Rivera, H. Woodworth, and R. W. Boyd, Phys. Rev. Lett. **129**, 133902 (2022).
[17] V. Parigi, V. D'Ambrosio, C. Arnold, L. Marrucci, F. Sciarrino, and J. Laurat, Nat. Commun. **6**, 7706 (2015).
[18] Y.-H. Ye, M.-X. Dong, Y.-C. Yu, D.-S. Ding, and B.-S. Shi, Opt. Lett. **44**, 1528 (2019).
[19] H. Hu, D. Luo, and H. Chen, Appl. Phys. Lett. **115**, 211101 (2019).
[20] C. Pan, C. Yang, H. Hu, J. Wang, Y. Zhang, Y. Qin, D. Wei, H. Chen, H. Gao, and F. Li, Opt. Lett. **46**, 5579 (2021).
[21] B. Ndagano, H. Sroor, M. McLaren, C. Rosales-Guzmán, and A. Forbes, Opt. Lett. **41**, 3407 (2016).
[22] M. McLaren, T. Konrad, and A. Forbes, Phys. Rev. A **92**, 023833 (2015).
[23] A. Selyem, C. Rosales-Guzmán, S. Croke, A. Forbes, and S. Franke-Arnold, Phys. Rev. A **100**, 063842 (2019).
[24] I. Nape, K. Singh, A. Klug, W. Buono, C. Rosales-Guzman, A. McWilliam, S. Franke-Arnold, A. Kritzinger, P. Forbes, A. Dudley *et al.*, Nat. Photonics **16**, 538 (2022).
[25] J. Ishihara, T. Mori, T. Suzuki, S. Sato, K. Morita, M. Kohda, Y. Ohno, and K. Miyajima, Phys. Rev. Lett. **130**, 126701 (2023).
[26] G. Milione, H. I. Sztul, D. A. Nolan, and R. R. Alfano, Phys. Rev. Lett. **107**, 053601 (2011).
[27] L. Margalit, M. Rosenbluh, and A. D. Wilson-Gordon, Phys. Rev. A **87**, 033808 (2013).
[28] M. Auzinsh, D. Budker, and S. Rochester, *Optically Polarized Atoms: Understanding Light-Atom Interactions* (Oxford University Press, New York, 2010).
[29] T. W. Clark, Sculpting shadows: On the spatial structuring of fields & atoms: A tale of light and darkness, Ph.D. thesis, University of Glasgow, 2016.
[30] S. Sharma and T. N. Dey, Phys. Rev. A **96**, 033811 (2017).
[31] H. R. Hamedi, V. Kudriašov, J. Ruseckas, and G. Juzeliūnas, Opt. Express **26**, 28249 (2018).
[32] Z. Li, S. Franke-Arnold, T. W. Clark, J. Wang, D. Zhang, and C. Wang, Opt. Express **30**, 19812 (2022).
[33] See Supplemental Material at http://link.aps.org/supplemental/10.1103/PhysRevLett.132.193803 for some details of the underlying theoretical calculations and experimental results.
[34] F. Castellucci, T. W. Clark, A. Selyem, J. Wang, and S. Franke-Arnold, Phys. Rev. Lett. **127**, 233202 (2021).
[35] S. Qiu, J. Wang, F. Castellucci, M. Cao, S. Zhang, T. W. Clark, S. Franke-Arnold, H. Gao, and F. Li, Photonics Res. **9**, 2325 (2021).
[36] N. Radwell, G. Walker, and S. Franke-Arnold, Phys. Rev. A **88**, 043409 (2013).
[37] $I \propto \exp\{-\alpha L\}$, where $\alpha$ is the absorption coefficient and $L$ the propagation distance. A logarithm yields the absorption $\propto \alpha L$.
[38] H. Li, V. A. Sautenkov, Y. V. Rostovtsev, G. R. Welch, P. R. Hemmer, and M. O. Scully, Phys. Rev. A **80**, 023820 (2009).
[39] S. Gao, F. C. Speirits, F. Castellucci, S. Franke-Arnold, S. M. Barnett, and J. B. Götte, Phys. Rev. A **102**, 053513 (2020).
[40] H.-J. Wu, B.-S. Yu, Z.-H. Zhu, W. Gao, D.-S. Ding, Z.-Y. Zhou, X.-P. Hu, C. Rosales-Guzmán, Y. Shen, and B.-S. Shi, Optica **9**, 187 (2022).
[41] C. Cisowski, C. Ross, and S. Franke-Arnold, Adv. Photonics Res. **4**, 2200350 (2023).
[42] S. K. Pal, and P. Senthilkumaran, Opt. Express **25**, 19326 (2017).
[43] J. Wang, Y. Chen, M. A. Al Khafaji, S. J. Svensson, X. Yang, C. Wang, H. Gao, C. M. Cisowski, and S. Franke-Arnold, Opt. Express **30**, 24497 (2022).
[44] A. McWilliam, C. Cisowski, Z. Ye, F. Speirits, J. Götte, S. Barnett, and S. Franke-Arnold, Laser Photonics Rev. **17**, 2300155 (2023).
[45] D. Zhang, T. Gao, P. Zou, L. Kong, R. Li, X. Shen, X.-L. Chen, S.-G. Peng, M. Zhan, H. Pu *et al.*, Phys. Rev. Lett. **122**, 110402 (2019).
[46] G. W. Henderson, G. R. M. Robb, G.-L. Oppo, and A. M. Yao, Phys. Rev. Lett. **129**, 073902 (2022).
[47] J.-Z. Li, C.-J. Zou, Y.-X. Du, Q.-X. Lv, W. Huang, Z.-T. Liang, D.-W. Zhang, H. Yan, S. Zhang, and S.-L. Zhu, Phys. Rev. Lett. **129**, 220402 (2022).
[48] J. R. Torgerson, M. M. Schauer, S. K. Lamoreaux, and S. Gleyzes, J. Opt. Soc. Am. B **22**, 72 (2005).
[49] F. Stopp, M. Verde, M. Katz, M. Drechsler, C. T. Schmiegelow, and F. Schmidt-Kaler, Phys. Rev. Lett. **129**, 263603 (2022).
[50] L. Ye, L. Yang, X. Zheng, and S. Mukamel, Phys. Rev. Lett. **126**, 123001 (2021).